Atmospheric Environment 246 (2021) 117754

Contents lists available at ScienceDirect

Atmospheric Environment

journal homepage: http://www.elsevier.com/locate/atmosenv

The effects of air pollution sources / sensor array configurations on the likelihood of obtaining accurate source term estimations

Shai Kendler [a,b,*], Asaf Nebenzal [c], David Gold [d], Patrick M. Reed [d], Barak Fishbain [a]

[a] Dept. of Environmental, Water and Agricultural Engineering, Faculty of Civil & Environmental Engineering, Technion – Israel Institute of Technology 616, Rabin Hall, Haifa, 32000, Israel
[b] Environmental Physics Department, Israel Institute for Biological Research 24, Lerer St, Ness Ziona, 74100, Israel
[c] Department of Mathematics, Technion – Israel Institute of Technology, Haifa, 320003, Israel
[d] School of Civil and Environmental Engineering, Cornell University, Ithaca, NY, 14853-3501, USA

HIGHLIGHTS

- New metrics to assess the effect of air pollution sources/sensor array configurations on the accuracy of the source term estimation.
- The estimation is based on sensors' response to changes in the source term.
- The source term is estimated for several cases using a multiobjective search algorithm combined with an atmospheric dispersion model.

ARTICLE INFO

Keywords:
Air pollution
Environmental sensing
Source term estimation
Atmospheric dispersion model
Sensor placement
Multiobjective optimization

ABSTRACT

Estimating the source term in the case of multiple leaks using a sparse sensor array is a challenging task. Here, the effect of sensor array/leak configurations on the reliability of the source term estimation is studied using two new measures. The first describes the overall change in the sensor array response to different source terms. The second represents the effect of the source term on the readout of each sensor in the array. These measures are subjected to several model cases differing in sensor array/leak configurations. Then, the source term is estimated using a self-adaptive multiobjective evolutionary (MOEA) search algorithm combined with a gas dispersion model. The method searches for a set of leaks, each one of which has a typical emission rate and location that results in a minimal difference between the sensors' actual and computed pollution concentration. This objective, which is often used for source term estimation, is traded off against the second objective of maintaining a minimum number of active sources, which follows Occam's razor principle of parsimony. Analysis of the results obtained for these model cases suggests that the measures can be implemented as a design tool using a combination of computer simulation and field experiments before operational deployment.

1. Introduction

Industrial activities involve the use of numerous chemicals which are often harmful to humans and the environment at large enough doses. Preventing chemical emissions into the atmosphere is the best way to address this critical issue but because there is no way to guarantee fail-safe operations, toxic gases and vapors may be accidently released into the environment (Dobor, 2017), due to accidents, terrorist attacks or even during routine operations. The first line of defense in the case of a chemical leak is the detection of the plume, and mapping the contamination level in the environment. Rohi et al. developed a sensing system that utilizes miniaturized CO_2, NO_2, CO, NH_3, SO_2, PM, O_3 sensors that are mounted on drones (Rohi et al., 2020). One of the motivations for this study was to provide a detailed mapping of the pollutant concentrations to attempt to mitigate the contamination by capitalizing on the portability of drones. However, the limited (15 min) flight time and the complexity involved in continuous 24/7 operation of a drone fleet emerge as shortcomings. Moltchanov et al. reported measurements of air pollutants with a network of six miniature wireless multi-sensors in three urban sites. This Wireless Distributed

* Corresponding author. Dept. of Environmental, Water and Agricultural Engineering, Faculty of Civil & Environmental Engineering, Technion – Israel Institute of Technology 616, Rabin Hall, Haifa, 32000, Israel.
E-mail addresses: skendler@technion.ac.il, ikendler@gmail.com (S. Kendler), asaf.n@technion.ac.il (A. Nebenzal).

https://doi.org/10.1016/j.atmosenv.2020.117754
Received 6 March 2020; Received in revised form 23 June 2020; Accepted 29 June 2020
Available online 10 July 2020

Environmental Sensor Network (WDESN) can capture spatiotemporal concentration variations if properly calibrated. (Moltchanov et al., 2015), (Fishbainet al., 2017) Optical systems such as the Light Detection and Ranging (LIDAR) monitor pollutant concentration by recording laser light scattering and absorption. (Slavov et al., 2019), (Aharoni et al., 2015) Potentially, LIDAR systems can provide detailed pollution mapping but this depends on having a clear line-of-sight, which may be infeasible in populated or industrial sites. An alternative approach is to locate the source of the leak and the mass emission rate (i.e., source term), and use this as input in an atmospheric dispersion model to generate spatial dense pollution maps (Danuso et al., 2015). Estimating the source term in the case of multiple leaks is important not only for assessing the environmental impact but also to prioritize the mitigating actions. This prioritization is critical in the case of a complex industrial site where access to the leak source might be dangerous and require trained personnel.

Estimating a source term that consists of multiple leaks requires careful consideration of sensor placement to provide an accurate depiction of the contamination levels in the field. Lerner et al. (2019) formulated the deployment of a low-cost sensor network as an optimization problem. In their work, the network was comprised of two types of micro-sensing units that monitored ozone, NO, and NO_2 emissions. The optimal locations were found using an optimization process that identified the set of locations under resource constraints that maximized the overall utility of the sensor network. However, their method only evaluated land use and the topographic nature of the region of interest and disregarded temporal factors such as atmospheric conditions. To account for the temporal factors, Nebenzal and Fishbain (2017) developed an interpolation method to find source locations based on the pollution concentrations measured using chemical sensors and a Gaussian Air Pollution Dispersion Model (GAPDM); Allen et al. (2007) described the use of a genetic search algorithm combined with a Second-Order Closure Integrated Puff (SCIPUFF) dispersion model. This algorithm was validated on synthetic and mesoscale (5–25 km) field experiment data (Dipole Pride 26 field). The model computes the source term in the case of a single leak that emits the tracer gas for a short period (2 s). Hirst et al. (2013) located and estimated sources of methane emission using a Markov chain Monte Carlo algorithm based sensor measurements and GAPDM. Performance was validated using real airborne data from a 1600 km^2 area containing two landfills, and a 225 km^2 area containing a gas flare stack. Methane concentrations, together with atmospheric conditions, flight and GPS data, were continuously recorded. Pollution concentration is measured at 1 Hz at a ppb resolution. It is worthwhile noting that such fine-grained measurement provides valuable input for the source term estimation algorithm. Another approach to obtain detailed sensor data was described by Cui et al. (2004), who developed a fuzzy logic model implemented in a mobile sensor network. Their mobile sensor network was composed of a set of robots that monitor the pollution concentration and communicate using an ad-hoc wireless network. Each robot in this array chooses the next sampling point based on the information obtained by the other robots. This operation algorithm was designed to ensure that the sensors cover a large area; hence, providing detailed information needed to locate the source of the emission. Lamb et al. developed a mobile laser based system for source term estimation. This system measures the concentration of a tracer gas (SF_6) released at a known mass flow rate from the same location as the interrogated site. The source term is estimated by measuring the tracer concentration at several locations and comparing it to the methane concentration emitted from the interrogated site. The accuracy, using this method, for a single point source was ±15% and ±50% for a diffuse source with no need for meteorological information or an atmospheric dispersion model (Lambet al., 1995). Brantley et al. described a mobile sensing system to assess methane emissions from oil and gas production sites (Brantley et al., 2014). This system detects methane concentration in the air using an optical spectrometer. Since vast deployment of these instruments is impractical, the system is mounted on a vehicle that measures the gas concentration for 15–20 min at several locations, resulting in a detailed mapping of the gas concentration. The second stage consists of estimating the source term using the USEPA OTM33A method (EPA, 2015), which utilizes the measured gas concentration, wind speed and direction as input for a GAPDM to estimate the source properties.

The complexity involved in the process of source term estimation requires conducting field experiments in which the source properties are defined in advance, the meteorological conditions, and the sensors'-observed concentrations are recorded during the experiment. In order to account for the large variability involved in such measurements, these experiments must be repeated several times with different source term and sensor geometries. Platt et al. (2008), (Platt, 2009) carried out an elaborate experiment aimed at comparing different algorithms for source term estimation. The test was carried out by the US DOD and is referred to as the Fusing Sensor Information from Observing Networks (FUSION) Field Trial 2007. The experiment consisted of 81 trials involving a mixture of instantaneous and continuous releases from 1 to 4 sources of a tracer gas (propylene). The source was located upstream at various distances (50 m, 150 m, and 250 m) from the main sensor grid comprised of 100 photoionization detectors and an additional 20 ultraviolet ion collectors spread over a 500 m × 500 m square grid. The meteorological conditions, which are essential input for the source term estimation algorithm, were recorded during the experiments. The results of 104 different scenarios, including 40 cases with a single source, 40 with two sources, 16 with three sources, and 8 with four sources, were used to test different source term estimation algorithms. The comparison was performed by eight algorithm developer teams that tested fourteen source term estimation methods. These tests were conducted using different portions of the meteorological and sensor information to simulate realistic scenarios in which some of the information might be missing. Source location accuracies at short distances are usually lower than at long distances, and the discrepancy in emission rate can be as high as an order of magnitude. More details on the findings of this comparative study were presented by Platt and DeRiggi. (Platt and Deriggi, 2012), (Platt and DeRiggi, 2012) The results obtained in such complex experiments can be further used to provide a standard platform for future developments of source term estimations methods based on standard databases and use consensual terminologies and methodologies ("harmonization") (Hanna and Young, 2017).

Hutchinson et al. (2017) reviewed methods for source term estimation using static or mobile sensors. This review of over 150 references describes two main approaches to source term estimation: the first is based on optimization techniques and the second on probabilistic approaches. The main difference between these two approaches is that probabilistic methods account for uncertainties in the input to the model that yield a probability density function. By contrast, optimization methods do not take these uncertainties into account and generate a deterministic source term estimation.

Many of these statistical and optimization studies aim at minimizing the discrepancy between estimated and measured pollution concentrations. For example, Haupt et al. developed a single objective optimization technique based on a genetic algorithm for source term estimation. By adjusting meteorological data and the (single leak) source term, the algorithm minimizes the difference between the measured (using a chemical sensor) and computed (using an atmospheric dispersion model) pollution concentration ("cost function"). When the estimated source term is close to the real one, the cost function is at its minimum value since the measured and computed pollution concentration are similar (Haupt et al., 2011).

The success of these techniques depends on the ability of the sensor array to provide unambiguous information on the pollutant concentration in the air. In the case of multiple leaks, as the gas plumes propagate through the atmosphere, they expand and finally overlap. Hence, accurate source term estimation in such scenarios requires several sensors located close to the leaks, preferably at distances that are shorter than

the separation between leaks. However, in many cases, the locations, or even the possible locations of the leaks are unknown; hence, this type of sensor deployment is not possible, and dealing with such scenarios is likely to become a numerically intensive endeavor. An elegant backward estimation algorithm was proposed in a classic letter by Gifford (1959). The dosage at a given receptor point can be treated as an average of dosages weighted by the strength of different emission sources. Therefore, it is possible to treat this receptor as the point of origin and calculate the upwind directed concentrations according to the relative weight of the sources as a form of "backward estimation". In so doing, the computational complexity is reduced since one can avoid computing the gas dispersion from numerous possible sources that may exist in urban areas. While Gifford used the GAPDM, which can be handled by modern computers even for large numbers of sources, more sophisticated dispersion models are significantly more numerically cumbersome; thus making the backward estimation technique still useful. For example, Bieringer et al. (Bieringeret al., 2015) developed a method for fast source term estimation based on an iterative computation process. In their method, the first guess of the source term is obtained by backward estimation using the SCIPUFF dispersion model. This guess and meteorological variables are then interactively refined by forward-estimation using a Gaussian puff dispersion model. This algorithm was tested on experimental data from the FFT07 experiment, (Platt et al., 2008), (Platt, 2009) and provided similar accuracy as the SCIPUFF model using fewer computation resources. Cantelli et al. (2015) developed and a genetic search algorithm for the identification of multiple leak scenarios. Their simulations were conducted in a 1000 m × 1000 m × 50 m computer-simulated test site using a point source and a steady-state Gaussian dispersion model. Due to the gas plumes overlap, the maximum number of sources that could be resolved was up to three.

The study reported here describes two complementary measures to assess complexity arising from the existence of multiple leaks monitored with a sparse detector array and their effects on the source term estimation accuracy. The first estimates sensor array sensitivity to changes in the source term, i.e., the potential for detection. The second uses the variability between the sensor-observed concentrations in different cases to estimate the likelihood of identifying the nature of the change. The predictive power of these two measures is illustrated in several model cases using a self-adaptive evolutionary multiobjective search scheme for estimating the source term. Resolving this complex situation with a limited and fixed number of sensors may potentially result in more than one feasible solution where the number of leaks in each solution could be different. Solutions in which the number of leaks is low will be referred to as "simple" solutions. The search mechanism is designed to prefer the combination of accuracy and simplicity underlying the law of parsimony (Blumer et al., 1987). The search component of this work was conducted using the hyper-heuristic and self-adaptive Borg multiobjective evolutionary algorithm (SA-MOEA) (Burkeet al., 2013).– (Giuliani et al., 2018) The method's efficacy was evaluated in these model cases assuming well-calibrated but noisy sensors.

2. Methodology

2.1. Definitions

Let Ω be the region of interest. In the context of this study, Ω is the monitored industrial area. Let $\{S\}$ be the set of possible leakage sources, where each source, $s \in \{S\}$ is located in $\omega_s \in \Omega$ and for a specific time t, emits q_s[kg/second]. Similarly, the set $\{R\}$ is the set of sensors, where each sensor, $r \in \{R\}$, is located in $\omega_r \in \Omega$ and records a pollution concentration of $c_r \left[\frac{\mu g}{m^3}\right]$. The source locations, $\{\omega_s\}$ and emission rates, $\{q_s\}$ for all $s \in \{S\}$ are unknown, whereas the sensor locations, $\{\omega_r\}$ and recorded values, $\{c_r\}$, for all $r \in \{R\}$ are known. Let m_{sr} be the pollution transfer function of a dispersion model which associates sensor r's observed concentration, c_r, with the emissions of source s. Thus, the model's estimated contribution of source $s \in \{S\}$ to the pollution concentration in $\omega \in \Omega$, is given by:

$$\widehat{c}_{\omega} = \boldsymbol{m}_{s\omega} \cdot \boldsymbol{q}_s \mid \forall \omega \in \Omega,\ \forall s \in \{S\} \tag{1}$$

For multiple source scenarios, each sensor's observed concentration is the contribution of all sources; i.e.:

$$\widehat{\boldsymbol{c}}_{\omega} = \sum_{s} \boldsymbol{m}_{s\omega} \cdot \boldsymbol{q}_s \;\Big|\; \forall \omega \in \{\Omega\},\ \forall s \in \{S\} \tag{2}$$

Since each leakage source has its own specific parameters and location with respect to the sensors, the values of m_{sr} for each source-sensor combination are determined by the dispersion model. For the sake of simplicity at this stage of the study, it is assumed that the dispersion model and the meteorological data are accurate. Accounting for real-life fluctuations and missing data requires additional study.

Based on these notations, the goal is to find the optimal set {S*} that represents the most accurate characterization of the leak sources. The decision variables for this optimization problem are the emission rates, q_ω for all ω∈Ω. Thus, each location $\omega \in \Omega$ can host a source. The algorithm is designed to find the minimum number of active sources ($q_\omega > 0$) that can explain the sensor-observed concentration. In this work, pollution concentrations at a single time were considered with constant leak rates.

2.2. Computer-simulated test site

Computations were made in a computer-simulated 600 m × 600 m flat area, with a constant westerly wind and class C5 atmospheric stability. Leak rates ranged from 0 to 1000 kg/s from 9 possible locations, in which the gas exits were located 5 m above ground level. Note that assuming the known gas exit height simplifies the problem and is only suited for specific applications. To gauge the air pollution, a sparse WDESN was assumed in several configurations relative to the leaks at ground level. Fig. 1 depicts several configurations used in this study. Leaks are marked by full red circles, and sensors by hollow black circles. Fig. 1a depicts a nine-sensor arrangement, where each sensor is located 50 m downwind from a leak. We dub this configuration "*Co9/9*". The leaks are 50 m apart. Fig. 1b shows a similar configuration as *Co9/9*, but with only six sensors, dubbed "*Co9/6*". Fig. 1c and d depict a line source, represented by a set of leaks in a straight line. In these configurations, six (Fig. 1c) and nine (Fig. 1d) sensors are located 50 and 65 m apart 50 m downwind, and are dubbed "*l9/6″* and "*l9/9″* respectively. The configurations in the figure are the "base layouts". To study the distance effect, the entire sensor array was shifted downwind (positive offset) or upwind (negative offset); zero offset was the "base layout".

Note that while there were nine possible leaks, some could have a zero kg/s leak rate and be inactive. These synthetic configurations were selected to test the method's capabilities and limitations. The application of this method to other sites will thus require adaptations, which are presented below. The assumed air-pollution contribution, c_r, in location r in the region of interest (ROI), of leak $s \in S$, with a leak rate of q_s, over the ROI, was computed using the GAPDM, assuming continuous release and a steady state (Ermak, 1977). More details on this model are provided in the supplementary material.

The computer-generated configurations presented in Fig. 1 depict well-defined situations. Studying these configurations by changing the sensor to leak distance, or the number of leaks may provide insights into other possible configurations. The *'l9/9'* configuration at the base layout and nine leaking sources represent a case with some gas plume overlap since the leak separations (50 m) are equal to the leaks-to- sensors distance. Increasing this distance also increases the gas plume overlap at the sensing points. On the other hand, reducing the number of active leaks reduces the gas plume overlap. The *'l9/6'* is similar to the *'l9/9'*, but decreasing the number of sensors means they have to be placed off the central axis of the gas plume, which makes it a less favorable

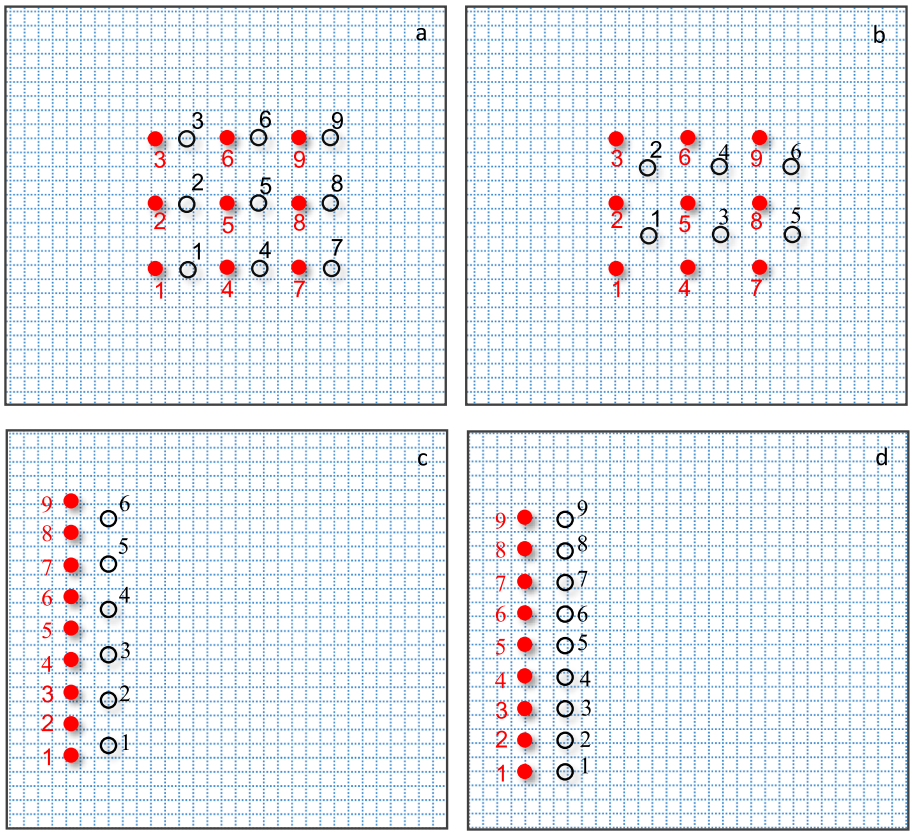

Fig. 1. Typical source (red dots and numbers) sensors (black circles and numbers) layouts. Note that the term "leak" refers to both active and non-active leaks; a) nine leaks/sensor pairs arranged in a compact group. Each sensor is located 50 m downwind from a source of emission; sources are 50 m apart ("Co9/9″), b) similar to Co9/9 using six sensors ("Co9/6), c) nine sources deployed in a line 50 m apart and a line of six sensors 50 m downwind; sensors are 65 m apart ("L9/6″), d) same as L9/6 using nine sensors; each sensor is lined up with one of the sources ("L9/9″). (For interpretation of the references to color in this figure legend, the reader is referred to the Web version of this article.)

situation. In the base layout, the *'Co9/9'* is a relatively convenient configuration. Increasing the separation between the sensors and leaks complicates this situation, as does decreasing the number of sensors such that (the *'Co9/6'* configuration) would be less optimal.

In addition to these well-structured configurations, some computations were performed in randomly generated sources-sensors setups. Each such configuration differs in one (or more) of the following parameters: number of sensors, number of active leaks, the average distance between two leaks (*'DL-L'*), the distance between the sensor and leak (*'DS-L'*) and the sensor offset from the center of the gas plume (*'offset'*). In all randomly generated cases, the locations of the leaks are randomly selected. If one has some prior knowledge on the site he can improve his network's performance by selecting sensors locations with reduced distances and offsets to the potential sources, i.e., leaks. Accordingly, situations in which one has some knowledge regarding the test site are stimulated by randomly selecting the reduced offsets and distances in a preferred small range. The absence of such knowledge is simulated by removing any constraint regarding the sensors' locations.

2.3. Measures of scenario complexity

As discussed above, estimating the source term in the case of multiple leaks is problematic, especially when the resulting gas plumes overlap (Gifford, 1959).– (Cantelli et al., 2015) Resolving such overlaps requires a dense network of sensors. However, the operational complexity of large WDESNs increases with the size of the network (Kizelet al., 2018) so that reducing the number of sensors without sacrificing accurate estimation of the source term is important. Hence, two new criteria were derived to provide a quantitative measure of the complexity of a scene, as follows:

1. Pairwise Euclidean Difference *(PED)* between the sensor network's calculated pollution concentrations for two different source terms (different leak locations and mass flow rates) while keeping all other problem parameters constant. The PED values depend on the maximum possible leak rate assigned to each source. Hence, the PED values were normalized to the maximal gas leak rate and are presented in ppm/kg/second.
2. Sensor Array Reading Correlation *(SARC)*; i.e., the Pearson correlation between the sensor network's calculated pollution concentrations for two different source terms (different leak locations and mass flow rates).

In subsection 2.6, considerations regarding real-world sensing data are provided in detail.

2.3.1. PED formulation

For {S'} and {S''}, two sets of active leaks; i.e., $\{S^{'}\} \neq \{S^{''}\}$, the PED as a function of {S}',{S}" is given by (3):

$$PED_{\{S^{'}\},\{S^{''}\}} = \sqrt{\sum_{r=1}^{|R|}\left(C_r^{\{S^{'}\}} - C_r^{\{S^{''}\}}\right)^2} \tag{3}$$

In the case of a source comprised of multiple leaks, there are many possible combinations of individual leak rates. Hence, the distribution of the PED values obtained for 10,000–20,0000 randomly selected source terms is presented. Typically, PED values drop as the change in the number of active sources declines. Hence, cases where the following transitions may occur were examined:

$$\{S\}_8^{'} \rightarrow \{S\}_8^{''},\ \{S\}_9^{'} \rightarrow \{S\}_9^{''},\ \{S\}_9^{'} \rightarrow \{S\}_8^{''},\ and\ \{S\}_8^{'} \rightarrow \{S\}_9^{''}$$

where $\{S\}_n^{'}$ represents a situation with *'n'* active sources with different leak rates. Note that the PED value in the case of $\{S\}_n^{'} \rightarrow \{S\}_n^{''}$ is not equal to zero in most cases since the specific leak rates can vary.

2.3.2. SARC formulation

Similarly, the $SARC_{\{S\}',\{S\}''}$ is computed (4):

$$SARC_{\{S'\},\{S''\}} = \rho\left(\vec{C}^{\{S\}'},\ \vec{C}^{\{S\}''}\right) \quad (4)$$

where $\vec{C}^{\{S\}'}$ is a vector of the sensors'-observed concentrations obtained for the source term {S}' and $\vec{C}^{\{S\}''}$ for {S}''.

2.3.3. Data obtained from the PED and SARC

Computing the PED results in an estimate of the difference in the total pollutant concentration measured by the sensors for different source terms. This is useful when estimating the capability of the sensor array to detect this type of change (sensitivity). Consider for example the simplest case in which the sensors are placed upwind. In this case, all the sensors'-observed concentrations are equal to zero regardless of the nature of the source term. Similarly, in the *L9/6* configuration the number of sensors (six) is lower than the number of possible leaks (nine); hence during the measurements the sensors are off the central axis of the pollution plumes. We will see later that this kind of sensor placement results in a low PED value compared to the *L9/9*. The SARC provides additional information regarding the observed concentration of each sensor in the array (specificity) for different source terms. If the correlation between the sensor-observed concentration for two different source terms is high, the information fed into the search algorithm may not suffice for reliable source term estimation. Fig. 2 shows the relationship between the SARC value and the number of active leaks (leaks having a mass-flow rate greater than zero). The computation, in this case, was performed by randomly selecting $\{S\}'_n$ *and* $\{S\}''_{n-1}$ (n = 1–9) and calculating the distribution of the computed *SARC* value. It shows that decreasing the number of leaks shifted the SARC distribution towards lower values since, in these conditions, there is a relatively large separation between the leaks. As the leak separation relative to the sensor distance increases, the amount of overlap between the gas plumes is reduced, resulting in reduced SARC values. The largest effect was obtained for the *L9/6* configuration but was considerably smaller for the *L9/9* and *Co9/9* configurations. Possible implementations are discussed in the section on optimization results.

2.4. Optimization problem formulation

Optimization was expressed through two formulations: a bi-objective formulation that traded off simplicity and accuracy, and a tri-objective formulation that traded off simplicity with the two accuracy objectives of under- and over-estimation. The tri-objective formulation is aimed at enhancing the search performance by providing additional input to the search algorithm in terms of both the magnitude of the error and its direction.

2.4.1. Bi-objective formulation

The bi-objective formulation was designed to solve the following minimization problem:

$$\{S^*\} = \min_{\{S\}} \mathbf{F} \quad (5)$$

where

$$\boldsymbol{F} = \begin{bmatrix} \Psi_{\text{error}} \\ |S^*|_0 \end{bmatrix} \quad (6)$$

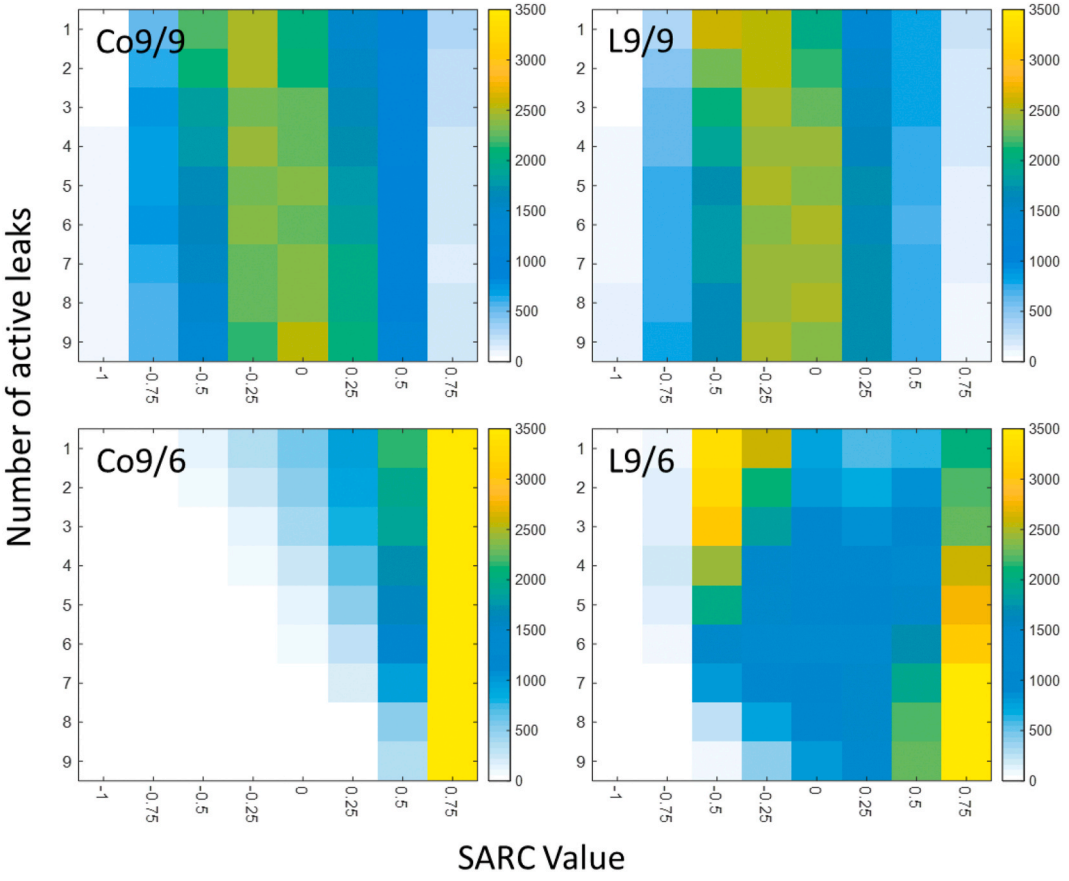

Fig. 2. The effect of the number of active leaks on the distribution of SARC values for various pollution source/sensor configurations. Number of counts for each SARC value are presented on the color scale. (For interpretation of the references to color in this figure legend, the reader is referred to the Web version of this article.)

F is a vector-based objective function, $\{S^*\}$ is the optimal set of sources (the source term), Ψ_{error} is the accuracy of the source term estimation and $|S^*|_0$ is the number of active leaks in $\{S^*\}$.

The minimization of the first objective, Ψ_{error}, is achieved by minimizing the discrepancies between the actual values measured by the sensors and the estimated values of the model:

$$\Psi_{error} = \sum_{r\in\{R\}} \left| c_r - \sum_{s\in\{S\}} m_{sr} \cdot q_s \right| \tag{7}$$

This objective is counterbalanced by the second objective, which is formulated on the basis of Occam's razor, and aims to find the minimal number of sources that can explain the recorded values, $C_r \forall r \in R$; i.e., the minimum number of active leaks, and $|S|_0$ symbols the number of active leaks (Donoho's ℓ0-"norm").

Formulating the problem as a multiobjective optimization provides an additional dimension to conventional search algorithms that are only aimed at providing the most accurate solution; i.e., minimizing the discrepancy between the computed and observed concentration (Ψ_{error}). This dimension needs to be added given the high number of possibilities in the case of multiple leaks. Cantelli et al. (2015) addressed this issue by using an inverse model and by assuming a known number of sources. The formulation presented here utilizes an alternative approach that prefers solutions that decrease the error by a significant value ("epsilons" – see subsection 2.6) that is defined by the user according to the application specifics. Hence, solutions that introduce a non-significant improvement in the error function by adding more sources are rejected. The formulation presented here utilizes solutions with fewer active leaks (these solutions are referred to as "simple"). Consider, for example, a situation in which the sensors' observed concentrations exhibit large fluctuations regardless of the source term. Clearly, decreasing the discrepancy between the computed and observed concentration below these naturally occurring fluctuations is impractical. During a search this means that there are two possible solutions: S_n - a solution with 'n' active leaks, and S_{n+1} with 'n+1′ active leaks, Sn+1 is accepted if it reduces (Ψ_{error}) by a significant value ("epsilons" – see subsection 2.6), that is set by the user according to the application specifics, such as the pollution concentration fluctuations.

2.4.2. Tri-objective formulation

A variant of the bi-objective function is the tri-objective function in which the error objective function, Ψ_{error}, is divided into two parts: positive errors (over-estimation where-the computed concentration is higher than the observed one), and negative errors (under-estimation where the computed concentration is lower than the observed one). Note that these over- and underestimations are not a result of sensor operation (false negative or false positive alarms), but rather result from improper assignment of the mass-flow rate during the optimization. The purpose of this formulation is to guide the search algorithm towards the right solution by providing the Borg MOEA optimization algorithm with information on both the magnitude and direction of the error in its search for the optimal solution. The tri-objective minimization problem, in which Ψ_{error}, is split into two error terms takes the following form:

$$\{S^*\} = \min_{\{S\}} \mathbf{F} \tag{8}$$

$$\boldsymbol{F} = \begin{bmatrix} \Psi_{error<0} \\ \Psi_{error>0} \\ |S|_0 \end{bmatrix} \tag{9}$$

where **F** is the vector-based objective function, $\{S\}$ is the optimal set of sources, $|S|_0$ is the number of active leaks in $\{S\}$, $\Psi_{error<0}$ and $\Psi_{error>0}$ are of the sum of the under- and over-estimation errors from set $\{S\}$:

$$\Psi_{error<0} = \sum_{r\in\{R\}} \left| c_r - \sum_{s\in\{S\}} m_{sr} \cdot q_s \right|, \forall \left(c_r - \sum_{s\in\{S\}} m_{sr} \cdot q_s \right) < 0 \tag{10a}$$

$$\Psi_{error>0} = \sum_{r\in\{R\}} \left| c_r - \sum_{s\in\{S\}} m_{sr} \cdot q_s \right|, \forall \left(c_r - \sum_{s\in\{S\}} m_{sr} \cdot q_s \right) > 0 \tag{10b}$$

2.5. Multiobjective optimization

Both formulations described in equation (3) -(10) depict NP-hard problems, where there is no polynomial time-efficient solution. This accounts for the use of the Borg MOEA (Donoho, 2006). The Borg framework is a hyper-heuristic global (Burkeet al., 2013), multiobjective search tool that uses internal feedback during the search to dynamically adapt an ensemble of search operators (or strategies) by rewarding those that maximize search progress (i.e., the dominance of newly generated solutions).

The Borg MOEA initiates search for the optimal set $\{S\}$ by starting with a uniform random generation of its initial population of candidate solutions. Then the algorithm projects the set $\{S\}$ on Ω ; i.e., Eq (2), and evaluates the discrepancies from the measured values using the error function shown in Equation (7). Then, based on the two objectives ($|S|_0$ and Ψ_{error}), the Borg MOEA rewards those sets of decision variables $\{S\}$ that dominate the competing alternatives (i.e., those that are better on both objectives) until a high-quality approximation of the Pareto frontier is attained. Borg combines several algorithms: ε-dominance (Reed et al., 2007), ε-progress (Iwema et al., 2017), randomized restart (Martí et al., 2013), (White, 2018) and auto-adaptive multi-operator recombination (Gu et al., 2015), (Hadka and Reed, 2015) into a unified framework that has proven convergence (Hadka and Reed, 2013), (Laumanns, 1984), (Rudolph and Agapie, 2000). The approximate set, $\{S^*\}$, in each iteration was refined using the following internally competing genetic mating and mutation operators: Simulated Binary (SBX) (Ercan and Goodall, 2016), Patent-Centric (PCX) (Bi et al., 2016), Unimodal Normal Distribution (UNDX) (Gu et al., 2015), and Simplex (SPX) (Jain and Srinivasulu, 2004), crossovers as well as Differential Evolution (DE) (Andrews et al., 2011), and Uniform Mutation (UM) (Pelletier et al., 2006). The Borg MOEA auto-adapts the probability of which genetic operators to use according to the operators' offspring's success rate in previous iterations. To avoid a convergence of the algorithm to a local minimum, a stochastic restart mechanism exploiting Uniform Mutation is built into the BORG MOEA to automatically detect and avoid premature convergence to a local optimum and to achieve a diverse set of solutions (Burkeet al., 2013).

To account for the effects of the MOEA's stochastically generated initial parameters, a multiobjective search was run 10 separate times, where each run contained a different random seed (sample of initial parameters). Each random seed was run for up to 500,000 function evaluations. The Borg MOEA performance has been found to be primarily controlled by the number of function evaluations (NFE) the algorithm executes (Hadka and Reed, 2012). Runtime diagnostics were performed on all seeds to ensure the 500,000 NFE used in this study was adequate to approximate the Pareto frontier. The runtime performance of each seed was measured using the hypervolume (Zitzler et al., 2003) (Knowles and Corne, 2002), a metric that computes the volume of the objective space dominated by a set of solutions which provides a measure of both the diversity and proximity of the approximation set. The hypervolume was calculated every 100 function evaluations and tracked across the MOEA search. Runtime diagnostic results indicated that the NFE was sufficient (see supplementary information). The final Pareto approximate set reported here is the reference set of non-dominated solutions across all 10 random seeds.

The significant precisions ("epsilons") for Ψ_{error} were 1 ppb (both for the bi- and tri-objectives error objective functions) and 0.5 for $|S|_0$.

Borg's default values were used for all other search and permutation parameters (see (Hadka and Reed, 2012) for further details). The typical runtime was less than a minute when using this set of execution parameters. In cases where computation resources are limited, note that these parameters can be refined to meet the specific challenges and requirements of the problem at hand.

2.6. Methodology for real-world applications

The method presented in this work is based on a Gaussian dispersion model which requires minimal computing resources compared to other models such as for example the Lagrangian, (Oettl et al., 2005), (Shai kendler) computational fluid dynamic (CFD) (Li et al., 2006), CALPUFF (Levy et al., 2002), and AERMOD, (Cimorelliet al., 2005). However, these models may provide better accuracy for specific applications. Using the method presented here with another dispersion model requires additional research and perhaps some modifications. Choosing the best dispersion model should take the terrain topography, size, number of possible leaks, number of available sensors, required accuracy, and available computing resources into account. An example appears in Park and Seok who developed a methodology for selecting an appropriate dispersion model using several fuzzy inferential statistical measures that were integrated into a single index to evaluate dispersion models to predict ground-level SO_2 concentration in coastal areas (Park and Seok, 2007).

Sensors of various types are also available that differ in terms of their specificity with respect to the material of interest, the minimum detectable level (MDL) and dynamic range (DyR). Once the pollutant dispersion in the target site has been modeled, the expected pollutant concentrations in different scenarios can be estimated. Using these data, the efficacy of a specific sensor to provide an accurate estimation of the pollutant concentration in the air can be evaluated. The number of sensors and their placement are also critical factors that should be taken into consideration.

Although increasing the number of sensors will have a positive impact on the accuracy of the results (Thomaset al., 2018), it will also increase the operational cost. Hence this work focused on the case of a constant small number of sensors that were placed downwind. In real cases, more sensors need to be deployed to account for wind variations. Another issue to consider is the measurement noise in an outdoor environment, such as an industrial site. Somov et al. developed gas sensors for industrial sites, but even these ruggedized sensors must be calibrated periodically (Somov et al., 2013). Nodop et al. conducted atmospheric experiments involving the controlled release of Perfluorocarbon tracers (PFC) into the atmosphere. By measuring the PFC concentration, dispersion through the atmosphere was studied (Nodop et al., 1998). They showed that when using a calibrated gas chromatograph, the concentration of the tracer could be measured at an accuracy of 2.7–14.2%. For the current study, a photoionization detector (PID) was used to compare our theoretical findings to possible real-life sensing performance. This detector's MDL was sub-PPM, and its DyR spanned three orders of magnitude, which enabled the study of a wide range of emission rates. After calibration, the detector was found to be accurate ($R2 = 0.982$) and responded to pollution in real time (seconds) (Golbabaei et al., 2012). Hence, it possible to obtain a 1–2 min average of the sensor-observed concentration to reduce the fluctuations. Thus, an overall noise level of 15% of the entire sensor array is a fair estimate for assessing the performance of this method. It is worth noting that such meticulous calibration and maintenance are highly demanding. Hence, studying the trade-offs between sensor performance and source term estimation accuracy is essential.

Once the problem is characterized in detail, the PED and SARC values can be computed for several configurations in order to select the most favorable one. The performance can be then tested in this configuration by simulating several scenarios, as described in the next sections.

3. Results

3.1. Scenario complexity estimation

Fig. 2 shows the Pairwise Euclidean Difference between the sensor network's calculated pollution concentrations (PED - see section 2.3) value distribution for several sensor/leak-source configurations in the "base layout". Fig. 4 shows the PED value distribution for several sensor/leak source configurations as a function of the offset from the base layout as shown in Fig. 1. For the *Co9/9*, *L9/9*, and *L9/6* arrangements, the PED values peaked at the base layout. The PED values for the *Co9/9* and *L9/9* were similar and higher than for the *L9/6* and *Co9/6* layouts. In the *Co9/6*, in the base layout, the sensors were placed off the central axis of the gas plume; hence, the PED values increased with the offset as the gas plumes expanded. At high offset values, the PED values converged to a similar value in all cases (~40–80 ppm/kg/second) indicating that the gas plume was almost homogeneous at this distance, and that the sensor-observed concentrations were independent of the leak configuration. Hence, the preferred location to compute the source term was at short distances. From the perspective of using the PED as a design tool, if one takes the *Co9/9* base layout configuration at a leak rate that varies from 0 to 1 kg/s, the most probable PED value is 1200 ppm/kg/second. If using a PID sensor array having a sub-ppm detection limit with a wide linear range, this assessment shows that such detectors may provide reliable input to the search algorithm. A trickier question is how specific these changes are to the nature of the source. One measure of this specificity is the SARC, since a low SARC value indicates that the sensor-observed concentrations are specific to each situation and can provide a sound basis for the source term estimation. Fig. 5 shows the computed Sensor Array Reading Correlation (SARC – see section 2.3) values obtained at different configurations as a function of the offset from the base layout. It shows that in the base layout, the SARC values for the *L9/9* configuration were low in most cases, and the most probable SARC value was zero. Only 26% of the SARC values exceeded zero. The *Co9/9* configuration appeared to be similar to the *L9/9*, and 36% of the SARC values exceeded zero due to the overlap of gas plumes. Increasing the offset of the sensor array up to 225 m in the case of the *L9/9* configuration only had a slight effect on the SARC values. The SARC values in the *Co9/9* were very sensitive to the offset. Once the detectors were placed outside the leak area, the overlapping of the gas plumes resulted in high SARC values. The SARC values for the *Co9/6* configuration were high for all offset values due to the mismatch between the sensor and gas plume locations. Similarly, the SARC values for the *L9/6* configuration were high in the base layout due to the mismatch between the sensor locations and the gas plumes. As the offset increases, the pollution plumes expand and can be detected by the sensors, resulting in the shifting of the SARC value distribution towards lower values.

Using the PED and SARC values shows that the *L9/9* configuration was the simplest case to resolve, and that the *Co9/*9 would be slightly more challenging. Resolving the *Co9/6* configuration was the most challenging. The data from the *L9/6* configuration were mixed: the most probable PED value was 400 ppm/kg/second, which was twenty times higher than that of the *Co9/6* and three times lower than that of the *L9/9* configuration. The SARC values closer to the base layout were close to one. This made it hard to predict whether determining the source term in this configuration was possible. Hence, studying this configuration can shed light on the relationships between the SARC and PED measures; i.e., which of these measures can provide more information to determine the source term in different configurations. The results depicted in Figs. 2–5 were obtained for well-defined configurations, but exploring more scattered configurations resulted in similar conclusions as to the effect of gas plume overlap, the number of sensors and the leak-to-sensor distance on the PED and SARC values.

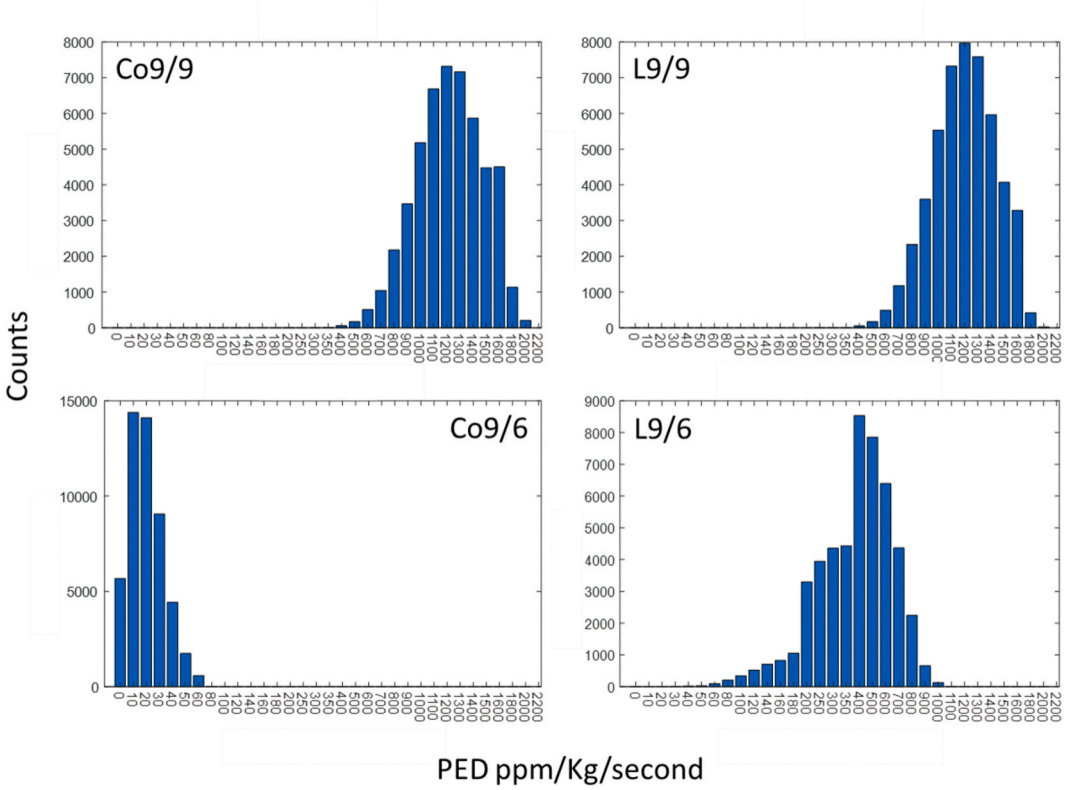

Fig. 3. Pairwise Euclidean Difference value distributions for several sensor/leak configurations (indicated in each figure).

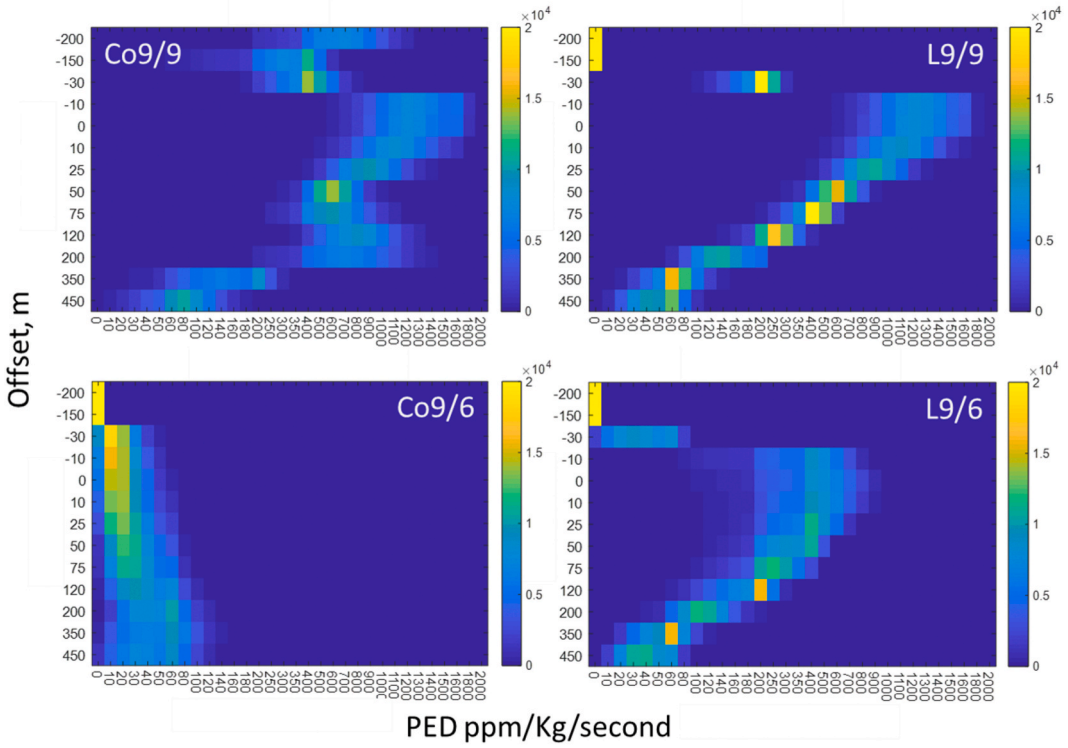

Fig. 4. Pairwise Euclidean Difference (PED) value distributions for several configurations (indicated in each figure) as a function of the offset distance from the base layout as presented in Fig. 1. Number of counts for each PED value are presented using the color scale where high values are depicted in warm yellows and low counts are in cold blues. (For interpretation of the references to color in this figure legend, the reader is referred to the Web version of this article.)

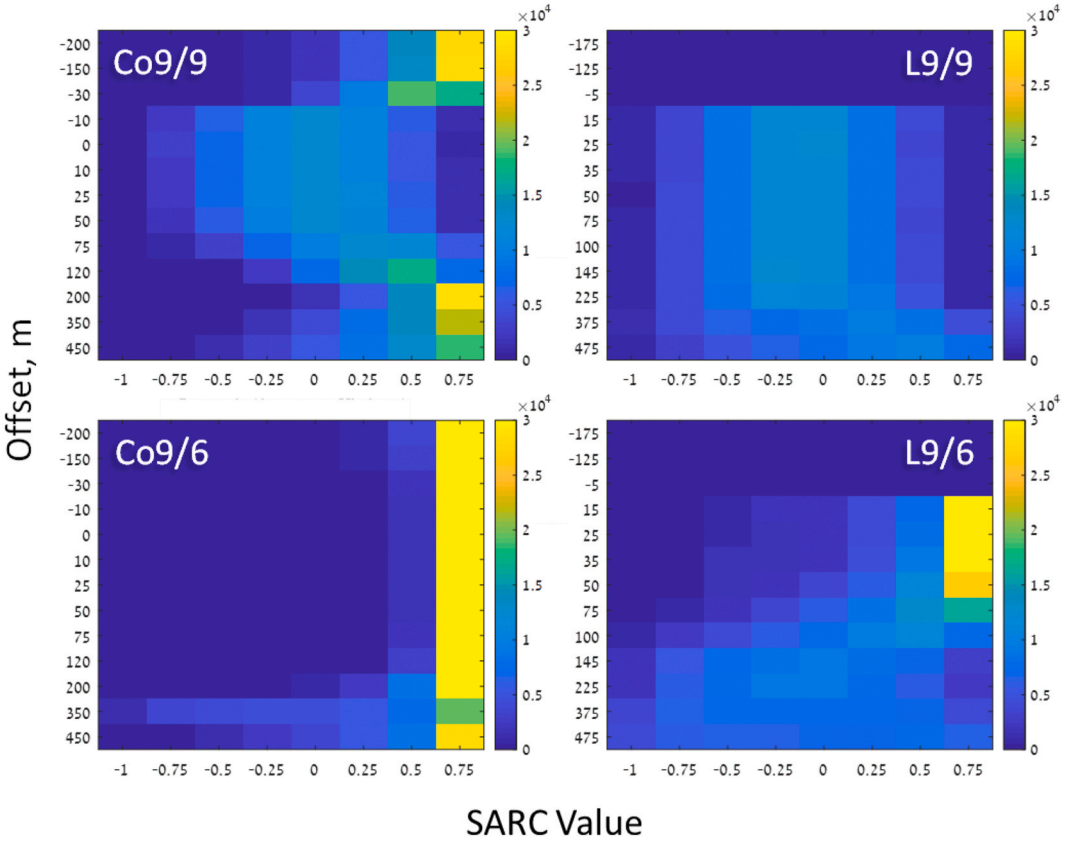

Fig. 5. Sensor Array Reading Correlation (SARC) values for various configurations (indicated in each figure) as a function of the offset. SARC values are presented using the color scale - high values are depicted in warm yellows and low counts in cold blues. (For interpretation of the references to color in this figure legend, the reader is referred to the Web version of this article.)

3.2. Source term estimation using Bi-objective function

Fig. 6 shows the Pareto frontiers calculated by the Borg for the *Co9/9* configuration in the base layout for increasing numbers of leaks, $|S|_0 = \{1,\cdots,9\}$. The x-axes in each of the graphs depict the calculated value of Ψ_{error}. The y-axes represent the number of active sources for a given solution. The x-axis error bars represent 15% noise in the sensor-observed concentration. The minimum Ψ_{error} was achieved for the correct number of leaks in each scenario. However, in real cases, even with meticulously calibrated sensors, the observed concentration noise is likely to bias the search process. This effect is expected to influence the search outcome if $|S|_0>6$, since the improvement in Ψ_{error} above this value is comparable to the error induced by sensor noise. Thus estimating a source with '*n*' active leaks requires '*n*' ideal sensors with zero noise that are located close to the leaks downwind. Adding even a small amount of noise reduces the performance. In this case, assuming a ±15% level limits the number of resolvable leaks to six when using nine sensors. Further increases in sensor noise level or wind fluctuations will require adding more sensors. If adding more sensors is impossible, one should consider repeating the search several times. In each search a slightly different sensor-observed concentration is be fed into the search algorithm, which may result in a different $|S|_0$ value. In this fuzzy situation, the decision-maker needs to implement a predetermined policy. The safest plan is to act under the assumption that the maximal computed $|S|_0$ value is the actual one ("Safety Driven Policy" SDP). If resources to respond to many leaks are limited, responding to the lowest computed $|S|_0$ value ("Resource Driven Policy" RDP) makes sense. Clearly in such a complicated situation, the situation will not be resolved in one step. Regardless of the decision-maker's policy, the efforts to estimate should continue after some of the leaks have been fixed. In this case repeating the estimation will be simpler since repaired leaks can be ignored in the search process. This approach might provide a more accurate source term estimation especially in cases in which reducing the number of active leaks reduces the SARC value, as shown in Fig. 2.

These results can be further analyzed by investigating the leak rates generated by Borg and comparing them to the preset leak rates. Fig. 7 compares the preset leak rates (on the x axis) to the calculated leak rates (on the y axis) having the minimal Ψ_{error} in several configurations with different $|S|_0$. The plots show that the calculated and actual leak rates were in excellent agreement. In realistic cases, this level of accuracy may not be feasible and probably not required. The decision-maker can best take advantage of this calculation if, instead of the exact numerical value for the leak rate, a three-level system is implemented that provides categories such as 'high' (leak rate = 1000-500 kg/s), 'medium' (leak rate = 500-100 kg/s) and 'low' (leak rate = 100-0 kg/s). This type of approach can serve to prioritize the response to the leaks. Analyzing the *L9/9* configuration yielded similar results.

The case for the *Co9/6* configuration (Fig. 1b), is more complicated, as predicted by both the PED and SARC values. In this configuration, minimizing Ψ_{error} did not result in an accurate estimation of $|S|_0$ or the leak rates (Fig. 8). Examining the results more closely revealed that the estimate of the leak rates from sources located on the west side of the tested area (1–3) was accurate (marked by arrows in Fig. 8b).

Thus far, the results have supported the hypothesis that determination of the source term is possible in sensor/leak configurations having large PED values and low SARC values such as the *Co9/9* and the *L9/9* configurations. In configurations such as the *Co9/6,* the sensors are placed off the central gas plume axis, resulting in low PED and high SARC values which make the estimation of the source term impossible. Similarly, configurations such as the *L9/9* and the *Co9/9* may be resolved if the sensors are placed close to the base layout, as can be seen from the PED that depended on the offset values (Figs. 4 and 5). The *L9/*

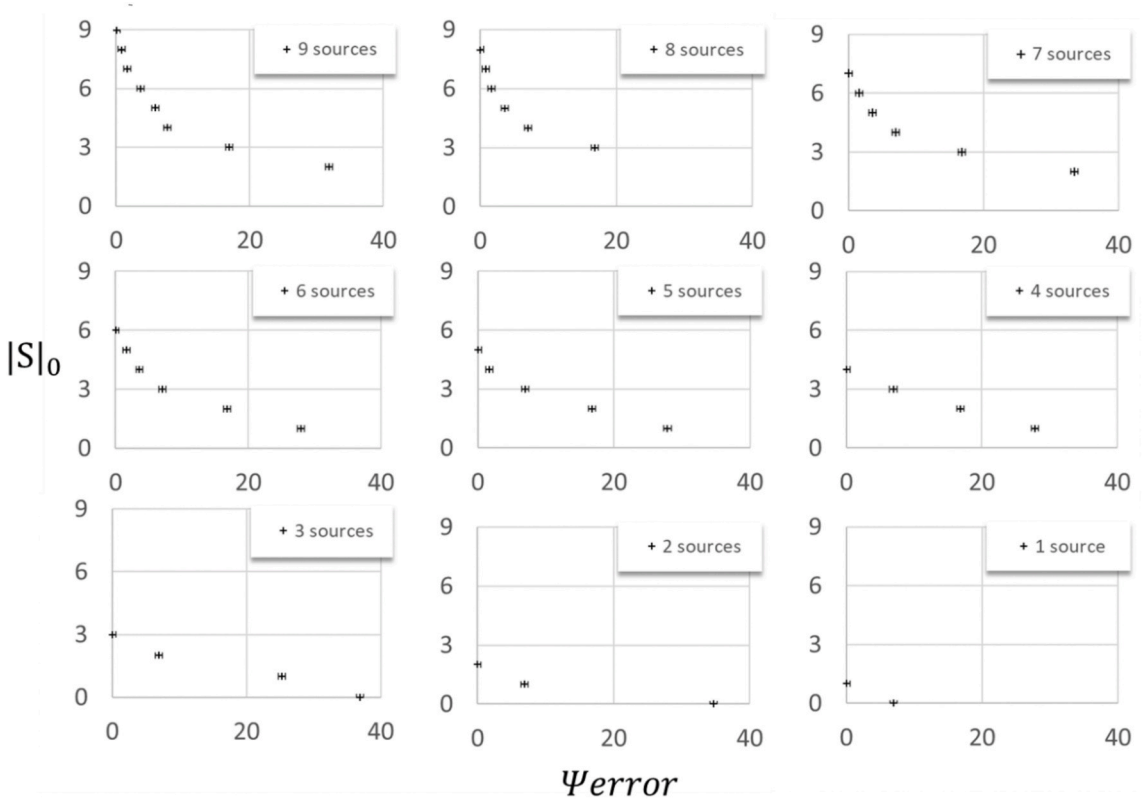

Fig. 6. Pareto frontiers calculated for the Co9/9 layout for several $|S|_0$ using the bi-objective function. The x-axis error bars represent 15% noise in the sensor observed concentration.

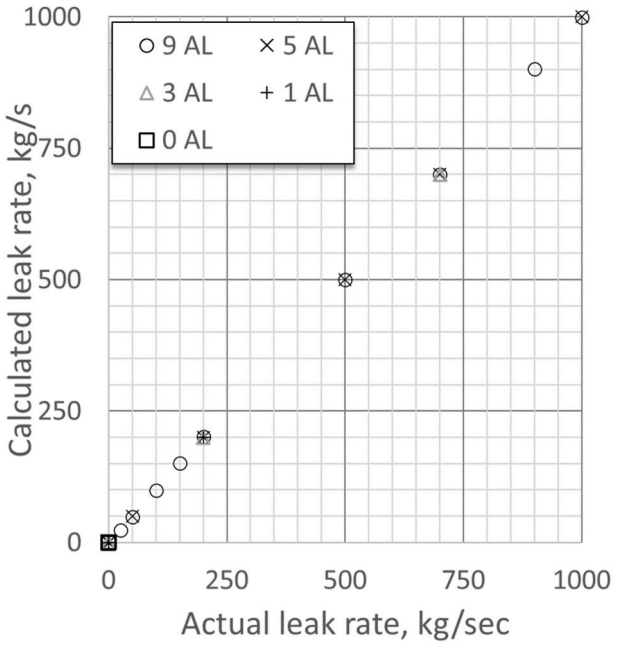

Fig. 7. Comparison of the calculated vs. actual mass flow rates for source terms with a different number of leaks with a mass flow greater than zero ("active leaks" – "AL"). The number of active leaks used in each calculation is presented with different symbols – see graph legend.

6 configuration was particularly interesting in that the indications obtained from the SARC and the PED measure were contradictory (see next section).

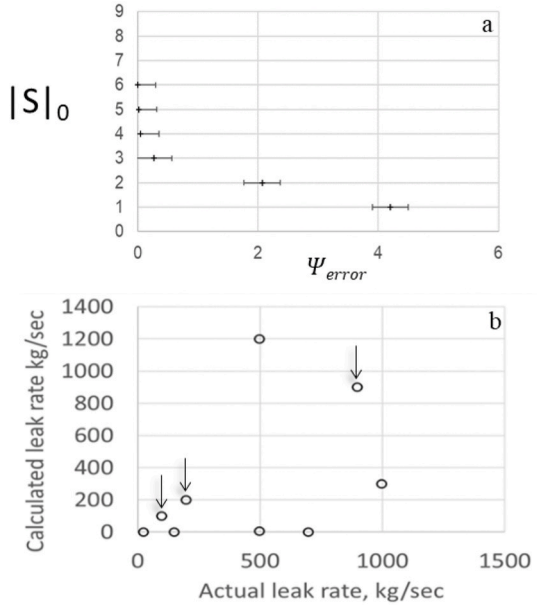

Fig. 8. a) Pareto frontier and b) comparison of the calculated vs. actual leak rate in the Co9/6 configuration for $|S|_0 = 9$. The x-axis error bars represent 15% noise in the sensor-observed concentration.

3.3. Improved search strategy using a tri-objective function

Several computations were carried out in the *L9/6* configuration for different sets of $|S|_0$ values. The accuracy of the computation for $|S|_0 > 4$ was poor. Therefore, an alternative search strategy was used that implemented the tri-objective function. Fig. 9 shows a comparison of the

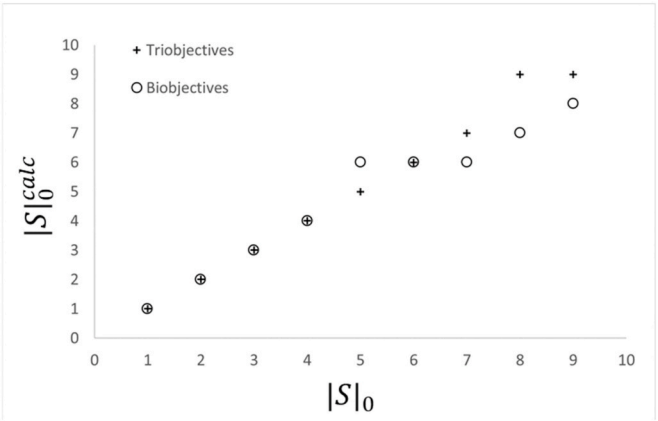

Fig. 9. Comparison of the actual ($|S|_0$) vs. the calculated ($|S|_0^{Calc}$) number of leaks using the bi-objective and tri-objective functions for the L9/6 configuration in the base layout.

actual $|S|_0$ to the calculated $|S|_0$ at a minimal value of the Ψ_error ($|S|_0^{Calc}$), using both the bi-objective and tri-objective functions. It indicates that in most cases, using the tri-objective function resulted in a more accurate estimation of $|S|_0$, compared to the bi-objective function. Out of nine cases, the tri-objective function estimated $|S|_0$ accurately in eight cases, compared to five cases successfully resolved by the bi-objective function.

Similar attempts to use the tri-objective formulation with the complex *Co9/6* configuration were unsuccessful. The improvement in the *L9/6* configuration was due to the fact that the search algorithm exploited feedback on both the direction and the magnitude of the error. This additional information guided the search algorithm to a more accurate result in most cases. These findings suggest that resolving a configuration having large SARC values is problematic even with high PED values. Limited success is obtained by enhancing the search process. It is worth noting that increasing the distance between the sensors and the leaks further decreased the accuracy for both the bi-objective and tri-objective formulation due to gas plumes overlap at larger distances. Resolving a configuration having both large SARC and low PED values such as the *Co9/6* configuration is impossible regardless of the search process.

3.4. Method evaluation in randomly-computer-generated test sites

The method has been evaluated using the tri-objective function in randomly-computer-generated sources-sensors test configurations. The two main parameters studied are the accuracy of the total mass flow rate and the probability of accurately determining the number of active leaks.

Fig. 10, shows the effect of the number of sensors, placed at a zero offset and 25–50 m downwind from nine active leaks (reduced distance = 0.5–3), on the method's accuracy. Note that each data point reflects the average of the computation results of over 100 tests configurations in which the leaks' locations are randomly selected. It shows that decreasing the number of sensors while keeping nine active leaks reduces the method's performance. The best situation is when the number of sensors is equal to the number of active leaks. In such a case, the average error is ~12%, and the probability to accurately determine the number of active leaks is 80%.

Reducing the number of sensors significantly decreases the method's performance; for example, when using eight sensors, the probability to accurately determine the number of active leaks is only 35%, and the error of the computed mass-flow rate is 50%. Hence it is concluded that the number of sensors should be equal or higher than the number of active leaks. Similar computations were performed when keeping the number of sensors constant (nine) and randomly choosing the number of active leaks and their locations. The method's performance improves as the number of active leaks is reduced. The average computed mass flow error was below 5% when the number of active leaks is lower than five.

The effect of the reduced offset and distance has been estimated in randomly generated configurations, having nine active leaks and nine sensors (Fig. 11).

It shows that moving away from the center of the gas plume has a significant effect on the accuracy of the mass flow rate at the extreme the computed mass-flow rate error varies between 25 and 250% (Fig. 11a). In this range of reduced offset values, the probability to accurately determine the number of active leaks varies between 80 and 100% (Fig. 11b). Keeping the reduced offset at zero and increasing the reduced distance decreases the method's performance due to the overlap of the gas plumes. In this range of reduced distances, the mass flow rate estimation error varies between 20% and 120% (Fig. 11c) and the probability of accurately determine the number of active leaks decreases from 1, in short distances, to 0, in longer distances (Fig. 11d).

The above computations describe situations in which the leaks are randomly placed in the computer-generated test site, and the sensors are placed using some knowledge regarding the possible locations of the leaks and the wind direction. The method is robust to changes in the sensor-leak distance as long as the reduced distance is 0.5–1 provided that the offset values are small, i.e., the locations of the sensors are close to the center of the gas plume. Such knowledge regarding the interrogated site may be limited in some cases. The performance of the method under these situations, were performed without using any prior knowledge. These computations showed that the source term estimation accuracy in such situations is low. For example, the probability to accurately estimate S0 is 0.6 and 0.48 when the number of active leaks is

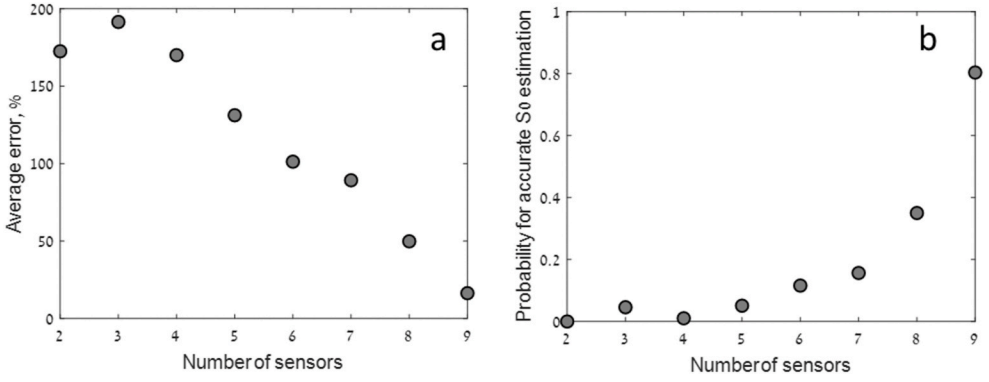

Fig. 10. The effect of number of sensors on the calculated mass flow rate accuracy (a) and the probability to accurately estimate the number of active leaks (b). Number of active leaks is 9, reduced distance is 0.5–3, and offset = 0, total number of randomly-computer generated-test sites is n = 850.

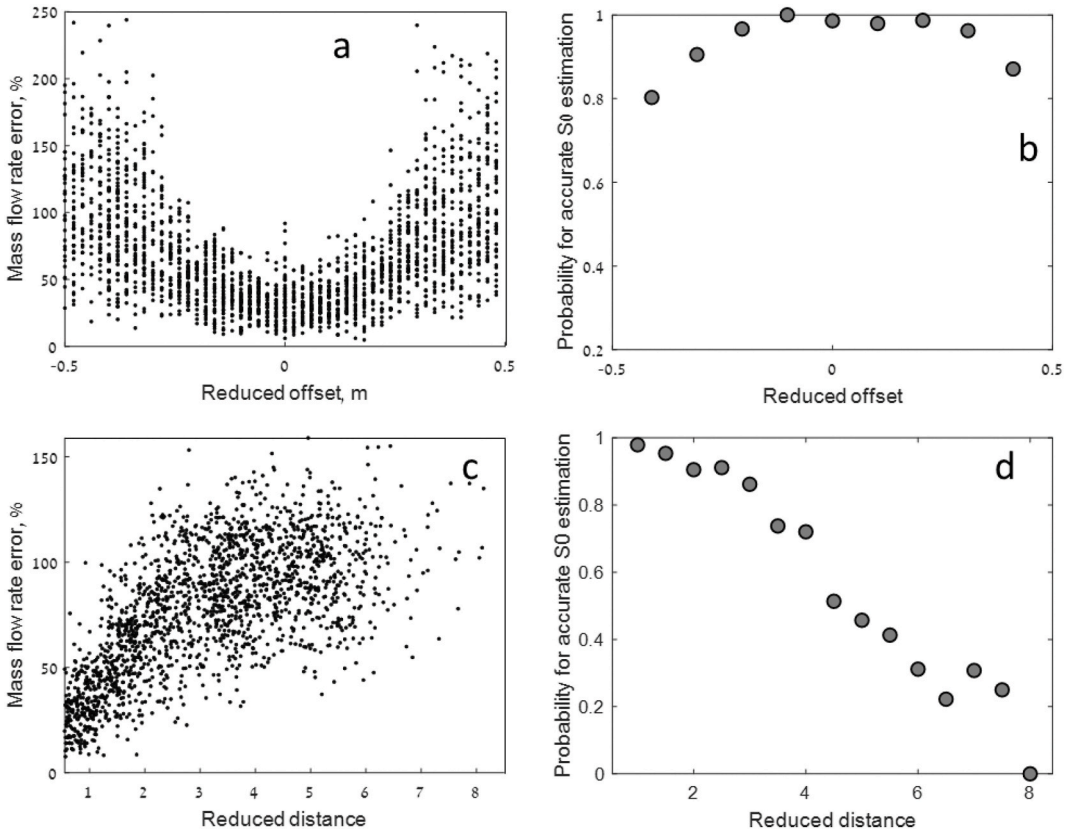

Fig. 11. The effect of the reduced-offset on the calculated mass flow rate accuracy (a) and the probability to accurately estimate the number of active leaks (b) at reduce distance of 0.5–1 ($D_{S\text{-}L}$ = 25–50 m). The effect of the reduced-distance on the calculated mass flow rate accuracy (c) and the probability to accurately estimate the number of active leaks (d) at reduce offset of 0, $D_{S\text{-}L}$ is varied between 25 and 300 m. Number of active leaks is and sensors is 9. Number of randomly-generated test sites is 2100 in each case.

one and two, respectively. The error in mass flow rate estimation is over 100%. Therefore, it is concluded that if one wants to utilize a sparse sensor array, some prior knowledge regarding the interrogated site is required. In the absence of such knowledge, one must deploy more sensors or to mount them on a moving platform.

4. Summary and conclusions

Detection of chemical leak locations and rates are crucial when attempting to define the appropriate mitigating response and when assessing the environmental impact. These objectives become more complex as the number of leaks increases, especially when the sensor network is sparse. The primary reason for this complexity is that as gas plumes propagate through the atmosphere, they expand and overlap. Two new measures were put forward here to estimate the likelihood of resolving a specific configuration of sensors/leaks. The first measure is the Pairwise Euclidean Difference between the observed pollution concentrations obtained with different source terms (PED). High PED values indicate that changes in the source term will result in a high change in the sensor-observed concentrations. The second measure, the Sensor Array Reading Correlation (SARC), accounts for the specific response of each sensor in the array. If for a certain source/sensor array configuration, the SARC value is low, the sensor observed concentrations are specific to every source term. In this case the information obtained from the sensors provide useful input to the source term estimation algorithm. Several distinct configurations were generated by computer simulations with different SARC and PED values, and were analyzed using a multi-objective optimization search. The optimization traded off two objectives: the error in gas concentration estimation, while minimizing the number of active leaks. Solutions having a low number of active leaks were considered "simple" solutions. Using simplicity as an objective adheres to Occam's razor principle of parsimony, which states that the simplest solution is most likely the right one. A variant of this formulation consists of three objectives: simplicity and the two error terms of over- and under-estimation. The resulting tri-objective formulation emerged as more successful than the bi-objective formulation in challenging configurations having high SARC and medium PED values. The method was also challenged with randomly-computer-generated configurations. It shows that the method is effective if the number of leaks is equal or lower than the number of active leaks and prior knowledge regarding possible leak location and wind direction is available. Resolving such a complex situation without such prior knowledge might be possible using more sensors or mounting them on a moving platform. The method is comprised of two modules: an optimization and an air pollution dispersion model. In the current work, the Gaussian atmospheric dispersion model was used. Future work will involve adapting a non-steady-state dispersion model, the Lagrangian model, to the method presented in this paper. A detailed study of the effect of sensor array attributes; i.e., the number of sensors, their minimum detectable level and dynamic range, quality of the calibration, noise, and placement. The methods developed in this study will then be validated using real data obtained in controlled experiments.

CRediT authorship contribution statement

Shai Kendler: Conceptualization, Data curation, Formal analysis, Investigation, Methodology, Software, Validation, Visualization, Writing - original draft, Writing - review & editing. **Asaf Nebenzal:** Formal analysis, Methodology, Software. **David Gold:** Data curation, Formal analysis, Methodology, Software, Validation, Visualization,

Writing - review & editing. **Patrick M. Reed:** Formal analysis, Methodology, Software, Validation, Writing - review & editing. **Barak Fishbain:** Conceptualization, Formal analysis, Funding acquisition, Investigation, Methodology, Project administration, Resources, Supervision, Writing - original draft, Writing - review & editing.

Declaration of competing interest

The authors declare that they have no known competing financial interests or personal relationships that could have appeared to influence the work reported in this paper.

Acknowledgments

This work was partially supported by the Israel Ministry of Science and Technology Research Program and the Israel Ministry of Environmental Protection.

Appendix A. Supplementary data

Supplementary data to this article can be found online at https://doi.org/10.1016/j.atmosenv.2020.117754.

References

Aharoni, R., Ron, I., Gilad, N., Manor, A., Arav, Y., Kendler, S., 2015. Real-time stand-off spatial detection and identification of gases and vapor using external-cavity quantum cascade laser open-path spectrometer. Opt. Eng. 54 (6) https://doi.org/10.1117/1.OE.54.6.067103.

Allen, C.T., Haupt, S.E., Young, G.S., 2007. Source characterization with a genetic algorithm-coupled dispersion-backward model incorporating SCIPUFF. J. Appl. Meteorol. Climatol. 46 (3), 273–287. https://doi.org/10.1175/JAM2459.1.

Andrews, F.T., Croke, B.F.W., Jakeman, A.J., 2011. An open software environment for hydrological model assessment and development. Environ. Model. Software 26 (10), 1171–1185. https://doi.org/10.1016/j.envsoft.2011.04.006.

Bi, W., Dandy, G.C., Maier, H.R., 2016. Use of domain knowledge to increase the convergence rate of evolutionary algorithms for optimizing the cost and resilience of water distribution systems. J. Water Resour. Plann. Manag. 142 (9) https://doi.org/10.1061/(ASCE)WR.1943-5452.0000649.

Bieringer, P.E., et al., Dec. 2015. Automated source term and wind parameter estimation for atmospheric transport and dispersion applications. Atmos. Environ. 122, 206–219. https://doi.org/10.1016/j.atmosenv.2015.09.016.

Blumer, A., Ehrenfeucht, A., Haussler, D., Warmuth, M.K., Apr. 1987. Occam's razor. Inf. Process. Lett. 24 (6), 377–380. https://doi.org/10.1016/0020-0190(87)90114-1.

Brantley, H.L., Thoma, E.D., Squier, W.C., Guven, B.B., Lyon, D., 2014. Assessment of methane emissions from oil and gas production pads using mobile measurements. Environ. Sci. Technol. 48 (24), 14508–14515. https://doi.org/10.1021/es503070q.

Burke, E.K., et al., 2013. Hyper-heuristics: a survey of the state of the art. J. Oper. Res. Soc. 64 (12), 1695–1724. https://doi.org/10.1057/jors.2013.71.

Cantelli, A., D'Orta, F., Cattini, A., Sebastianelli, F., Cedola, L., 2015. Application of genetic algorithm for the simultaneous identification of atmospheric pollution sources. Atmos. Environ. 115, 36–46. https://doi.org/10.1016/j.atmosenv.2015.05.030.

Cimorelli, A.J., et al., 2005. AERMOD: a dispersion model for industrial source applications. Part I: general model formulation and boundary layer characterization. J. Appl. Meteorol. 44 (5), 682–693. https://doi.org/10.1175/JAM2227.1.

Cui, X., Hardin, T., Ragade, R.K., Elmaghraby, A.S., 2004. A swarm-based fuzzy logic control mobile sensor network for hazardous contaminants localization. In: 2004 IEEE Int. Conf. Mob. Ad-Hoc Sens. Syst, pp. 194–203. https://doi.org/10.1109/mahss.2004.1392158.

Danuso, F., Rocca, A., Ceccon, P., Ginaldi, F., 2015. A software application for mapping livestock waste odour dispersion. Environ. Model. Software 69, 175–186. https://doi.org/10.1016/j.envsoft.2015.03.016.

Dobor, J., 2017. The importance of the teaching of case studies of industrial accidents in the disaster management education. Ecoterra—Journal Environ. Res. Prot. 14 (1), 26–32.

Donoho, D.L., Apr. 2006. Compressed sensing. IEEE Trans. Inf. Theor. 52 (4), 1289–1306. https://doi.org/10.1109/TIT.2006.871582.

EPA, 2015. Draft Other Test Method 33A: Geospatial Measurement of Air Pollution. Remote Emissions Quantifications - Direct Assessment, pp. 1–91.

Ercan, M.B., Goodall, J.L., 2016. Design and implementation of a general software library for using NSGA-II with SWAT for multi-objective model calibration. Environ. Model. Software 84 (October), 112–120. https://doi.org/10.1016/j.envsoft.2016.06.017.

Ermak, D.L., 1977. An analytical model for air pollutant transport and deposition from a point source. Atmos. Environ. 11 (3), 231–237. https://doi.org/10.1016/0004-6981(77)90140-8.

Fishbain, B., et al., 2017. An evaluation tool kit of air quality micro-sensing units. Sci. Total Environ. 575, 639–648. https://doi.org/10.1016/j.scitotenv.2016.09.061. September 2016.

Gifford, F.A., 1959. Computation of pollution from several sources. Int. J. Air Pollut. (2), 109.

Giuliani, M., Quinn, J.D., Herman, J.D., Castelletti, A., Reed, P.M., 2018. Scalable multiobjective control for large-scale water resources systems under uncertainty. IEEE Trans. Contr. Syst. Technol. 26 (4), 1492–1499. https://doi.org/10.1109/TCST.2017.2705162.

Golbabaei, F., Mortazavi, Y., Pourtaghi, G., Rismanchian, M., Foroushani, A., 2012. Evaluation of photoionization detector performance in photocatalytic studies for removing volatile organic compounds. Int. J. Environ. Health Eng. 1 (1), 42. https://doi.org/10.4103/2277-9183.102383.

Gu, F., Liu, H.L., Tan, K.C., 2015. A hybrid evolutionary multiobjective optimization algorithm with adaptive multi-fitness assignment. Soft Comput 19 (11), 3249–3259. https://doi.org/10.1007/s00500-014-1480-9.

Hadka, D., Reed, P., Sep. 2012. Diagnostic assessment of search controls and failure modes in many-objective evolutionary optimization. Evol. Comput. 20 (3), 423–452. https://doi.org/10.1162/EVCO_a_00053.

Hadka, D., Reed, P., May 2013. Borg: an auto-adaptive many-objective evolutionary computing framework. Evol. Comput. 21 (2), 231–259. https://doi.org/10.1162/EVCO_a_00075.

Hadka, D., Reed, P., 2015. Large-scale parallelization of the Borg multiobjective evolutionary algorithm to enhance the management of complex environmental systems. Environ. Model. Software 69, 353–369. https://doi.org/10.1016/j.envsoft.2014.10.014.

Hanna, S.R., Young, G.S., 2017. The need for harmonization of methods for finding locations and magnitudes of air pollution sources using observations of concentrations and wind fields. Atmos. Environ. 148 (November), 361–363. https://doi.org/10.1016/j.atmosenv.2016.11.008.

Haupt, S.E., Haupt, R.L., Young, G.S., 2011. A mixed integer genetic algorithm used in biological and chemical defense applications. Soft Comput. 15 (1), 51–59. https://doi.org/10.1007/s00500-009-0516-z.

Hirst, B., Jonathan, P., González del Cueto, F., Randell, D., Kosut, O., 2013. Locating and quantifying gas emission sources using remotely obtained concentration data. Atmos. Environ. 74 (October), 141–158. https://doi.org/10.1016/j.atmosenv.2013.03.044.

Hutchinson, M., Oh, H., Chen, W.H., 2017. A review of source term estimation methods for atmospheric dispersion events using static or mobile sensors. Inf. Fusion 36, 130–148. https://doi.org/10.1016/j.inffus.2016.11.010.

Iwema, J., Rosolem, R., Rahman, M., Blyth, E., Wagener, T., 2017. Land surface model performance using cosmic-ray and point-scale soil moisture measurements for calibration. Hydrol. Earth Syst. Sci. 21 (6), 2843–2861. https://doi.org/10.5194/hess-21-2843-2017.

Jain, A., Srinivasulu, S., Apr. 2004. Development of effective and efficient rainfall-runoff models using integration of deterministic, real-coded genetic algorithms and artificial neural network techniques. Water Resour. Res. 40 (4) https://doi.org/10.1029/2003WR002355.

Kizel, F., et al., Feb. 2018. Node-to-node field calibration of wireless distributed air pollution sensor network. Environ. Pollut. 233, 900–909. https://doi.org/10.1016/j.envpol.2017.09.042.

J. Knowles and D. Corne, "On metrics for comparing nondominated sets," in *Proceedings of the 2002 Congress on Evolutionary Computation*. CEC'02 (Cat. No.02TH8600), vol. vol. 1, pp. 711–716, doi: 10.1109/CEC.2002.1007013.

Lamb, B.K., et al., 1995. Development of atmospheric tracer methods to measure methane emissions from natural gas facilities and urban areas. Environ. Sci. Technol. 29 (6), 1468–1479. https://doi.org/10.1021/es00006a007.

Laumanns, M., 1984. Combining Convergence and Diversity in Evolutionary Multi-Objective Optimization, vol. 10.

Lerner, U., Hirshfeld, O., Fishbasin, B., 2019. Optimal deployment of a heterogeneous air quality sensor network. J. Environ. Informatics 34 (2), 99–107. https://doi.org/10.3808/jei.201800399.

Levy, J.I., Spengler, J.D., Hlinka, D., Sullivan, D., Moon, D., 2002. Using CALPUFF to evaluate the impacts of power plant emissions in Illinois: model sensitivity and implications. Atmos. Environ. 36 (6), 1063–1075. https://doi.org/10.1016/S1352-2310(01)00493-9.

Li, X.X., Liu, C.H., Leung, D.Y.C., Lam, K.M., 2006. Recent progress in CFD modelling of wind field and pollutant transport in street canyons. Atmos. Environ. 40 (29), 5640–5658. https://doi.org/10.1016/j.atmosenv.2006.04.055.

Martí, R., Resende, M.G.C., Ribeiro, C.C., 2013. Multi-start methods for combinatorial optimization. Eur. J. Oper. Res. 226 (1), 1–8. https://doi.org/10.1016/j.ejor.2012.10.012.

Moltchanov, S., Levy, I., Etzion, Y., Lerner, U., Broday, D.M., Fishbain, B., Jan. 2015. On the feasibility of measuring urban air pollution by wireless distributed sensor networks. Sci. Total Environ. 502, 537–547. https://doi.org/10.1016/j.scitotenv.2014.09.059.

Nebenzal, A., Fishbain, B., 2017. Hough-transform-based interpolation scheme for generating accurate dense spatial maps of air pollutants from sparse sensing. In: Environmental Software Systems. Computer Science for Environmental Protection, pp. 51–60.

Nodop, K., Connolly, R., Girardi, F., 1998. The field campaigns of the European tracer experiment (ETEX): overview and results. Atmos. Environ. 32 (24), 4095–4108. https://doi.org/10.1016/S1352-2310(98)00190-3.

Oettl, D., Sturm, P., Almbauer, R., May 2005. Evaluation of GRAL for the pollutant dispersion from a city street tunnel portal at depressed level. Environ. Model. Software 20 (5), 499–504. https://doi.org/10.1016/j.envsoft.2004.06.001.

Park, O.H., Seok, M.G., 2007. Selection of an appropriate model to predict plume dispersion in coastal areas. Atmos. Environ. 41 (29), 6095–6101. https://doi.org/10.1016/j.atmosenv.2007.04.010.

Pelletier, G.J., Chapra, S.C., Tao, H., 2006. QUAL2Kw - a framework for modeling water quality in streams and rivers using a genetic algorithm for calibration. Environ. Model. Software 21 (3), 419–425. https://doi.org/10.1016/j.envsoft.2005.07.002.

Platt, D., 2009. Nathanm Deriggi, "Comparative investigation of source term estimation algorithms using fusion field trial 2007 data. In: AMS Annual Meeting, p. J1.2.

Platt, N., Deriggi, D.F., 2012. Comparative investigation of source term estimation algorithms for hazardous material atmospheric transport and dispersion prediction tools. In: IDA Doc D-4048. July.

Platt, N., DeRiggi, D., 2012. Comparative investigation of Source Term Estimation algorithms using FUSION field trial 2007 data: linear regression analysis. Int. J. Environ. Pollut. 48 (1–4), 13–21. https://doi.org/10.1504/IJEP.2012.049647.

Platt, N., Warner, S., Nunes, S.M., 2008. Evaluation Plan for Comparative Investigation of Source Term Estimation Algorithms Using Fusion Field Trial 2007 Data, D-3488. *Institute for Defense Analyses*, pp. 224–229.

Reed, P., Kollat, J.B., Devireddy, V.K., 2007. Using interactive archives in evolutionary multiobjective optimization: a case study for long-term groundwater monitoring design. Environ. Model. Software 22 (5), 683–692. https://doi.org/10.1016/j.envsoft.2005.12.021.

Rohi, G., Ejofodomi, O., Ofualagba, G., 2020. Autonomous monitoring, analysis, and countering of air pollution using environmental drones. Heliyon 6 (1), e03252. https://doi.org/10.1016/j.heliyon.2020.e03252.

Rudolph, G., Agapie, A., 2000. Convergence properties of some multi-objective evolutionary algorithms. Proc. IEEE Conf. Evol. Comput. ICEC 2, 1010–1016. https://doi.org/10.1109/cec.2000.870756, 0.

B. F. Shai kendler, "A Method for Gas Leak Detector Array Deployment – Optimization of the Detectors Placement and Attributesle," *in preperatio*n.

Slavov, L., Iliev, M., Ilieva, R., Angelova, R., 2019. Lidar Monitoring of Air Pollution over Urban Areas Combined with In-Situ Sampling of Particulate Matter Lidar Monitoring of Air Pollution over Urban Areas Combined with In-Situ Sampling of Particulate Matter, vol. 414, pp. 8–11 no. January.

Somov, A., Baranov, A., Spirjakin, D., Spirjakin, A., Sleptsov, V., Passerone, R., 2013. Deployment and evaluation of a wireless sensor network for methane leak detection. Sensors Actuators, A Phys. 202, 217–225. https://doi.org/10.1016/j.sna.2012.11.047.

Thomas, G.W., et al., 2018. Low-cost, distributed environmental monitors for factory worker health. Sensors 18 (5), 1–17. https://doi.org/10.3390/s18051411.

White, J.T., 2018. A model-independent iterative ensemble smoother for efficient history-matching and uncertainty quantification in very high dimensions. Environ. Model. Software 109 (February), 191–201. https://doi.org/10.1016/j.envsoft.2018.06.009.

Zitzler, E., Thiele, L., Laumanns, M., Fonseca, C.M., Da Fonseca, V.G., 2003. Performance assessment of multiobjective optimizers: an analysis and review. IEEE Trans. Evol. Comput. 7 (2), 117–132. https://doi.org/10.1109/TEVC.2003.810758.